Potential-Induced Structural Change in a Self-Assembled Monolayer of 4-Methylbenzenethiol on Au(111)

Kyoungja Seo and Eric Borguet*

Department of Chemistry, Temple University, Philadelphia, Pennsylvania 19122

Received: July 15, 2006; In Final Form: October 14, 2006

Potential-induced structural change in a self-assembled monolayer (SAM) of 4-methylbenzenethiol (4-MBT) on Au(111) is investigated by in situ scanning tunneling microscopy (STM). STM images in 0.1 M $HClO_4$ indicate that a 4-MBT SAM on Au(111) consists of multiple phases in electrochemical environments. These phases include ordered domains (α-phase), aggregated molecular patches (β-phase), and potential dependent structures (β'-phase and γ-phase). At a potential positive of 0.3 V_{SCE}, comparable to the potential of zero charge (pzc) of Au(111), Ostwald ripening of α-phase domains is observed. Aggregated molecular patches are annealed, by the applied potential, to form a structured β'-phase. At a potential negative of 0.3 V_{SCE}, the structure of 4-MBT SAMs transforms to a new phase (γ-phase), 2.0 ± 0.5 Å higher than the surrounding α-phase surface. This is shown to be an STM tip-enhanced structural change, and is a consequence of the weak binding of thiol to gold at a potential negative of the pzc. Stepping the substrate potential back from 0.2 to 0.4 V_{SCE} transforms the γ-phase to the α-phase.

Introduction

Self-assembled monolayers (SAMs) of organothiols on gold surfaces are model systems, forming well-ordered 2D structures, to understand the fundamental properties of organic thin films and monolayers.[1−4] Aromatic thiols have an azimuthally anisotropic structure, that aligns the molecules through $\pi-\pi$ stacking,[5−8] and a higher electrical conductance compared to alkanethiols.[9,10] Aromatic thiols have been considered candidates for a number of applications including molecular wires and electron-transfer promoters for electroanalytical sensors.[9−11] To control and design the properties of the modified surface it is necessary to study the orientation and arrangement of self-assembled molecules at electrified interfaces. However, the nature and dynamic behavior of the self-assembly process of aromatic thiols, e.g., the number of monolayer phases and the thermodynamic stability of each phase, have been less studied compared to those of alkanethiols.

Ordered SAMs on Au(111) are believed to be the result of the van der Waals intermolecular interactions and the sulfur−Au interaction. Most long-chain alkyl and aromatic thiol SAMs form the $(\sqrt{3} \times \sqrt{3})$ structure consistent with close packing of sulfur on Au(111).[1] For example, the well-ordered $(\sqrt{3} \times \sqrt{3})$ structures of long-chain aromatic thiols on Au(111), such as oligophenylene thiols, terphenyl mercaptanes, and aromatic-terminated aliphatic thiols, have been observed by scanning tunneling microscopy (STM) measurements.[12−17] However, these are not the only structures observed. For example, $(2\sqrt{3} \times \sqrt{3})$ and $(5\sqrt{3} \times 3)$ structures were reported for biphenyl alkanethiols, $CH_3(C_6H_4)_2(CH_2)_nSH$ SAMs.[12] Yang et al. reported a striped $(7 \times \sqrt{3})$ phase for 2-phenylethanethiol on Au(111).[17] Baunach et al. observed benzylmercaptane with striped $(15 \times \sqrt{3})$ and $(2 \times \sqrt{3})$ structures on Au(111) in solution,[18] while a $(\sqrt{3} \times \sqrt{3})$ structure was reported by Tao et al. in air for the same molecule.[19] On the other hand, a theoretical study of benzenethiol adsorption suggested that the aromatic group energetically favors a herringbone arrangement with a $(2\sqrt{3} \times \sqrt{3})$ structure.[20] Clearly there are many different adsorption structures for aromatic thiols on Au(111) reflecting different surface coverages[12] and experimental conditions.[18]

In the case of short aromatic thiols, other interactions, e.g., between the benzene ring and surface,[11] between functional groups,[21] and the intermolecular $\pi-\pi$ interaction,[5,22] can drive the packing structure to deviate from the $(\sqrt{3} \times \sqrt{3})$ structure. Such strong intermolecular interactions, compared with the van der Waals lateral intermolecular interactions that drive *n*-alkanethiol molecules to assemble in well-defined monolayer structures, can drive the short aromatic thiols to form multilayers, preventing the observation of the ordered phase in STM measurements.[18] For example, a high-resolution STM image of a benzenethiol SAM with a $(\sqrt{13} \times \sqrt{13})$ structure was reported by Osawa et al.[23] In contrast, other STM studies concluded that benzenethiol cannot form an ordered structure.[13,17,19] Monolayers of 2- and 4-mercaptopyridine and bis(2- and 4-pyridyl)disulfide yielded a well-ordered structure with a $(p \times \sqrt{3})$,[5,11,24−28] while 2- and 4-aminothiophenol SAMs were imaged only as a few molecular rows instead of larger ordered domains.[21]

The chemisorption of adsorbates on metal surfaces can lead to a weakening of bonding between surface metal atoms or the bonding between surface and bulk metal atoms, resulting in higher metal adatom mobility.[29,30] The surface morphology of thiol modified gold can be influenced by the nature and dynamic behavior of thiolate−Au complexes. For example, the lower binding energy of sulfur to Au for arenethiols, compared with alkanethiols, can lead to less mobility of arenethiolate−Au complexes in the SAMs.[17] The binding energies of the sulfur atom to the Au atom for arenethiol and alkanethiol was estimated to be 46 and 74 kJ mol^{-1}, respectively.[17] The energies were estimated by subtracting the physisorption enthalpies of benzene and *n*-hexane[31,32] (i.e., 60 and 53 kJ mol^{-1}, respectively) from the binding energies of benzenethiol[33] and hexanethiol[34,35] to Au (i.e., 106 and 127 kJ mol^{-1}, respectively).[17] Upon

* Address correspondence to this author. Phone: (215) 204-9696. Fax: (215) 204-9530. E-mail: eborguet@temple.edu.

10.1021/jp064493r CCC: $37.00
Published on Web 04/11/2007

adsorption of aromatic thiols, such as benzenethiol and its derivatives, Au adatoms slowly diffuse out of the terraces, and Au adatom islands are observed as opposed to the depressions (Au vacancy islands) observed for *n*-alkanethiol SAMs.[17]

Thermally induced phase transformations can be attributed to the diffusion of alkanethiolate−Au complexes.[17,36,37] However, the weaker binding energy of the sulfur to Au in aromatic thiols, compared to *n*-alkanethiols, reduces the mobility of aromatic thiolate−Au complexes in aromatic thiol SAMs.[17] Clearly, the behavior of alkanethiol SAMs may not necessarily be useful in predicting aromatic thiol SAM behavior.

The adsorption and desorption of thiolates, as well as phase transformations of thiol SAM surface structures, have been suggested to be a consequence of potential-induced mobilization of surface gold atoms.[24,38,39] For example, Schweizer et al. reported a potential-induced surface transformation of ethanethiol SAMs on Au(100) accompanied by a change in adsorbate packing density, a consequence of a change in the substrate Au surface atom density.[38]

Conjugated molecular structures, such as aromatic thiols, are candidate components for molecular electronics.[10] To use aromatic thiols in such applications, we believe that insight into surface thermodynamics of the aromatic thiol SAMs under various environments is required. To date, potential-induced structural changes in only a few aromatic thiol SAMs have been reported, e.g., nitrobenzenethiol, mercaptopyridine, and bis-(pyridyl)disulfide.[22,24−26] Baunach et al. reported a phase transformation of 4-mercaptopyridine SAMs taking place at potentials close to the onset of reductive desorption, from the $(5 \times \sqrt{3})$ and $(10 \times \sqrt{3})$ structures to a dense $(\sqrt{3} \times 1)$ structure in 0.1 M H_2SO_4.[25] However, the electrochemical activity of the nitrobenzene group and the acidic hydrogen of the pyridinium group complicate our understanding of the role of intermolecular $\pi-\pi$ interactions.

We report the electrode-induced phase transformations in a simple aromatic thiol, 4-methybenzenethiol (4-MBT), self-assembled monolayer (SAM). The 4-MBT SAM on Au(111) was chosen to investigate the dynamic behavior of aromatic thiol SAMs, without the complication of any acid-based moiety[25] that might influence adsorbate mobility under the potential applied to the substrate electrode. In addition, cyclic voltammetry experiments show a lack of electrochemical activity for 4-MBT in the potential range from −0.25 to +0.65 V_{SCE}.

We observed and characterized a number of phases in the 4-MBT monolayer in an electrochemical environment. The thermodynamic stability of each phase was evaluated as a function of substrate potential, by time-lapse STM at potentials chosen to be negative and positive of the potential of zero charge (pzc), ∼0.3 V_{SCE} for Au(111) in acidic solutions.[40]

In addition to substrate potential-induced structural changes in a 4-MBT SAM, we report, for the first time to our knowledge, a tip potential-enhanced phase transformation of aromatic thiol SAMs.

In applications that employ STM tips to achieve nanoscale structural changes in SAMs, the tip electric field perturbs the molecular charge distribution and hence the sulfur−Au bond.[17,41,42] However, the local structural changes achieved to date, e.g., local desorption and phase transformation, were irreversible in alkanethiol SAMs.[43] Under electrochemical environments, it may be possible for the charge distribution of the sulfur−Au bond to be regulated by applying a potential, leading to more control of these effects.

Experimental Section

The Au(111) single-crystal disk (Mateck GmbH, Germany) was chemically cleaned by hot piranha solution (1:3 H_2O_2 (J.T. Baker, CMOS) and H_2SO_4 (J.T. Baker, CMOS)) (**Caution:** piranha solution is a very strong oxidant and is extremely dangerous to work with; gloves, goggles, and a face shield should be worn), followed by hydrogen flame annealing before use. Cyclic voltammetry of Au(111) in 0.1 M H_2SO_4 and $HClO_4$ (Fisher Scientific Co.) solutions was employed to evaluate the surface of the Au(111). All electrolyte solutions were prepared with purified water of 18.2 MΩ•cm (Barnstead, EasyPure with UV light). 4-Methylbenzenethiol (4-MBT) SAMs were prepared by immersing the Au(111) for 5 min or 20 h into a solution of 0.05−0.2 mM 4-MBT (Aldrich) in ethanol, followed by 1 min of utrasonication in ethanol to remove excess molecules from the surface. Cyclic voltammetry of 4-MBT SAMs modified Au(111) in 0.5 M KOH (Fisher Scientific Co.) was employed to estimate the surface concentration from the reductive desorption of 4-MBT molecules. All cyclic voltammetry was performed under a N_2 atmosphere after degassing electrolyte. STM imaging (Molecular Imaging, Picoscan 2100) was performed in 0.1 M H_2SO_4 and $HClO_4$ solutions under potential control provided by a bipotentiostat (Molecular Imaging, Picostat). Tungsten tips were electrochemically etched in 3 M KOH and then coated with paraffin wax to minimize the faradaic current occurring at the tip. All STM images were recorded in the constant current mode. The electrochemical cell was composed of an Au(111) working electrode and Pt wires as the reference and counter electrodes. All potentials are quoted versus the saturated calomel electrode (SCE).

Results and Discussion

STM Images. The samples were initially imaged in 0.1 M $HClO_4$ or H_2SO_4 solutions at a potential where the adlayer is electrochemically stable (e.g., 0.4 V). There were no noticeable differences in the images obtained in $HClO_4$ or H_2SO_4 solutions, contrary to previous studies of more complex aromatic thiol SAMs.[24,25] The ordered domains, typically 30−50 nm in diameter, are composed of striped structures (α-phase), whose orientations reflect the Au(111) threefold symmetry (Figure 1A). Aggregated molecular patches (*β*-phase), observed at α-phase domain boundaries, are generally higher (∼0.5 Å) than the ordered α-phase domains in the cross-sectional analysis (Figure 1). These aggregated molecular patches (*β*-phase) become more ordered (*β*′-phase) with time (inset in Figure 1). The height difference between ordered *β*′-phase and ordered α-phase domains is generally ∼1 Å.

Au adatom islands form after the chemisorbed thiol-induced lifting of the Au(111) reconstruction.[17] However, the height difference between the *β*-phase and the α-phase is much less than the height of monatomic gold islands (∼2.5 Å).[44] The *β*-phase coverage, as high as 35%, is higher than the 4.4% extra Au atoms resulting from the lifting of the reconstruction.[17,45] While ultrasonication of the modified Au(111) in an ethanol solution should remove most of the excess physisorbed 4-MBT molecules from the surface, e.g., multilayers, chemisorbed molecules can remain on the surface. This leads us to suggest that the *β*-phase is comprised of chemisorbed 4-MBT molecules, but not gold islands covered with 4-MBT.

We identify three distinct structures within different domains of the striped α-phase (Figure 1). The measured lattice constants, for the α-phase structures **I** and **II** (Figure 2A,B), are $a = 0.48 \pm 0.02$ nm and $b = 1.4 \pm 0.1$ nm, and the angle between lattice vectors is $87 \pm 2°$. This model results in a $(4 \times \sqrt{3})$ structure

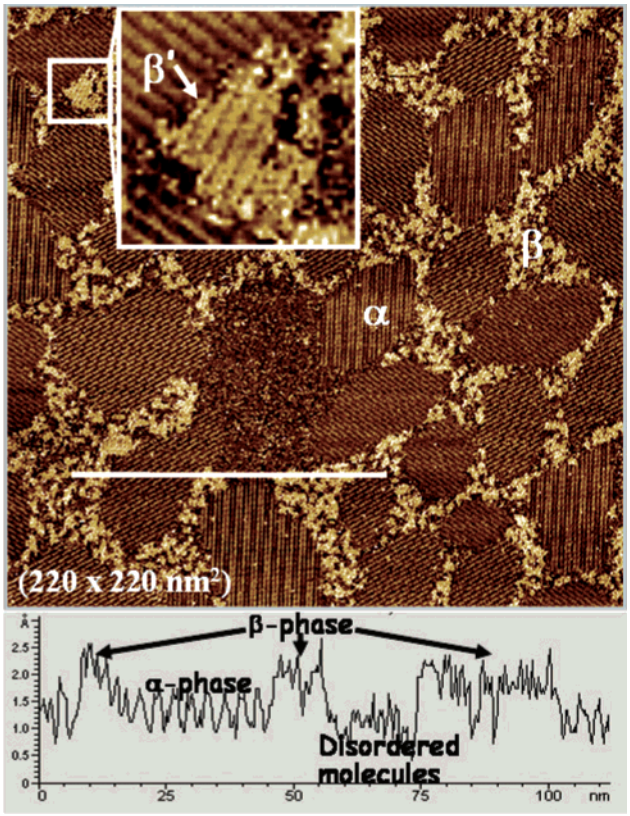

Figure 1. Typical STM image of the 4-MBT on Au(111) in 0.1 M $HClO_4$ at 0.4 V and cross-sectional analysis of the region marked by the line. The image shows striped structures (α-phase), aggregated molecular patches (β-phase), and ordered patches (β'-phase) (inset). The STM tip potential and tunneling current were 0.1 V and 0.6 nA, respectively. The 4-MBT SAM was prepared by immersion of Au-(111) in 0.05 mM ethanol solution for 5 min.

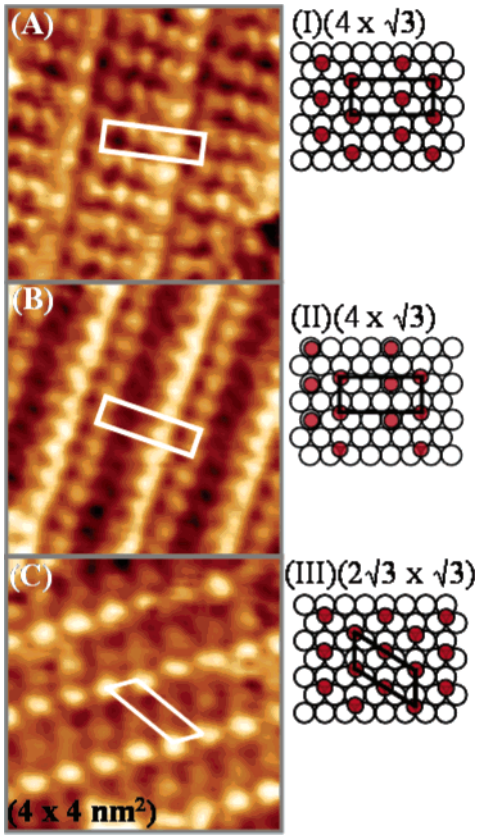

Figure 2. High-resolution STM images (α-phase) of the 4-MBT SAM on Au(111) in 0.1 M H_2SO_4 at 0.4 V and proposed models for three observed structures. Open circles represent the surface Au atoms. The sulfur headgroups are solid circles. The tip potential and tunneling current were 0.1 V and 0.4−0.6 nA, respectively. The 4-MBT SAM was prepared by immersion of Au(111) in 0.2 mM ethanol solution for 5 min.

($a = 4a_{Au}$, $b = \sqrt{3}a_{Au}$, where $a_{Au} = 2.89$ Å). The difference in the appearance of structures **I** and **II** is a consequence of the difference in adsorption sites; all molecules in structure **I** reside in 3-fold hollows, whereas molecules in structure **II** occupy both atop and 3-fold hollow sites.[5] The proposed unit cell corresponds to a coverage of 0.25 ML (0.35×10^{15} molecules cm^{-2}). For structure **III** (Figure 2C), the measured lattice constants are $a = 0.48 \pm 0.02$ nm and $b = 1.3 \pm 0.1$ nm, and the angle between lattice vectors is about $58 \pm 2°$. A possible model structure is a $(2\sqrt{3} \times \sqrt{3})$ structure. The proposed unit cell corresponds to a coverage of 0.33 ML (0.46×10^{15} molecules cm^{-2}).

Electrochemistry. The 4-MBT SAMs were electrochemically evaluated by cyclic voltammetry to determine the desorption potential. Cyclic voltammograms (CVs) of Au(111) covered with 4-MBT were recorded in 0.1 M $HClO_4$. The reductive desorption of 4-MBT on Au(111) starts at −0.25 V, which overlaps with the evolution of hydrogen (Figure 3). 4-MBT is not soluble in water and the desorbed molecules stay near the surface. The peak at 0.4 V in the anodic scan suggests readsorption of molecules. This is consistent with previous reports,[18,46] that electrochemically reductive desorbed thiolates can physisorb at the interface due to lack of solubility in aqueous solution, and that oxidative readsorption of physisorbed thiolates takes place in a subsequent reverse anodic scan. The cyclic voltammogram suggests that the 4-MBT SAM is electrochemically stable in the potential range between −0.25 and +0.65 V in 0.1 M $HClO_4$.

Cyclic voltammetry for the reductive desorption of 4-MBT on Au(111) was performed in 0.5 M KOH to obtain the surface concentration of adsorbed 4-MBT. The electrochemical desorption of *n*-alkanethiols from Au in alkaline solution was reported by Porter et al., and described as a one-electron reaction ($AuSR + 1\,e^- \rightarrow Au(0) + RS^-$).[47] The surface concentration of 4-MBT monolayers on Au(111) was determined from the reductive peak, and estimated to be about 7.5×10^{-10} mol cm^{-2} (0.45×10^{15} molecules cm^{-2}), corresponding to 72.3 C cm^{-2} of the charge under the peak, corrected for double layer charging. The corresponding local surface coverage is 0.33 ML with respect to the atomic density of Au(111). This value is high compared to the local surface concentration of some of the proposed surface structures. We suggest that aggregated molecules of the β-phase lead to a high charge estimation in CV for reductive desorption.[5,18]

Phase Transformation 1: Potential Annealing. Changes of the surface morphology, e.g., transformation from the β- to β'-phase, were monitored with time in 0.1 M $HClO_4$. At early times, just after the initial adsorption step, the β-phase dominates the surface (Figure 4A) and the striped α-phase domain, marked as a circle, exists inside the β-phase. To minimize mechanical drifts, the sample stage was usually stabilized in air for 2 h. Thus, the initial images show the disordered surface, and Figure 4A shows the result after several hours annealing in air without applied potential, i.e., before adding electrolyte.

On the other hand, in the image recorded 3 h later the surface mainly consists of striped α-phase domains, with the β'-phase occupying the domain boundaries (Figure 4B). The coverage of the β-phase is considerably reduced. Possible effects of STM

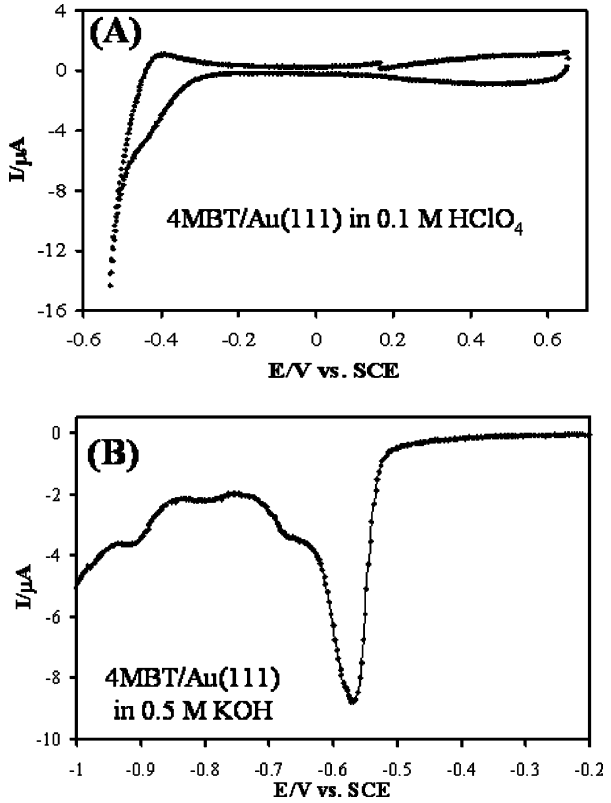

Figure 3. Cyclic voltammograms of the 4-MBT SAM on Au(111) in (A) 0.1 M $HClO_4$ and (B) 0.5 M KOH, respectively. Scan rate: 50 mV s^{-1}. The 4-MBT SAM was prepared by immersion of Au(111) in 0.05 mM ethanol solution for 5 min.

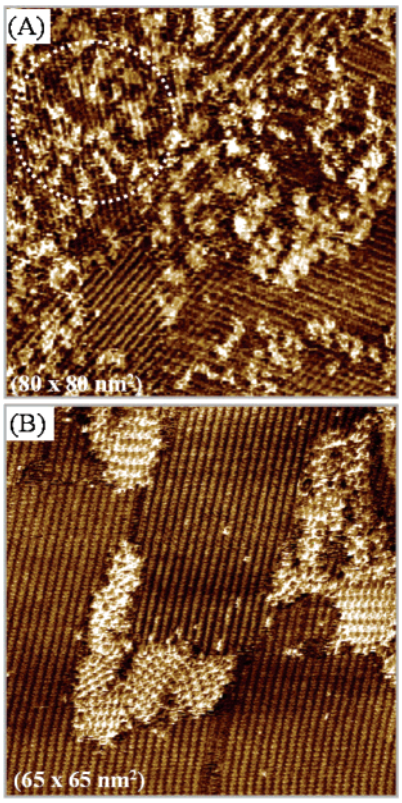

Figure 4. Surface structural change with a function of time of the 4-MBT on Au(111) in 0.1 M $HClO_4$ at 0.4 V. (A) At 23 min after the initial adsorption step, aggregated molecular patches predominate in the adlayer. The α-phase is mixed with the β-phase (white circle). (B) At 3 h after the initial adsorption step, the adlayer consists of the striped α-phase and the ordered β'-phase. The coverage of the β-phase is considerably reduced. The tip potential and tunneling current were 0.1 V and 0.6 nA, respectively. The 4-MBT SAM was prepared by immersion of Au(111) in 0.2 mM ethanol solution for 5 min.

tip scanning on the surface morphology are excluded as Figure 4B was imaged in a different part of the crystal surface from Figure 4A.

The proposed β'-phase structure, determined from images recorded after the sample was held at 0.4 V for 2−3 h with no scanning (Figure S1(A), Supporting Information), has lattice constants $a = 1.0 \pm 0.1$ nm and $b = 1.0 \pm 0.2$ nm, and the angle between lattice vectors is $91 \pm 2°$. A possible proposed model for the measured unit cell would fit best a (3×3) structure, corresponding to local coverage of 0.19 ML (0.27×10^{15} molecules cm^{-2}) (Figure S1(B),(C)).

Formation of ordered α-phase and β'-phase domains from the disordered β-phase suggests that 4-MBT molecules organize into ordered structures with time under electrochemical conditions. In addition, in the STM image obtained for the monolayer formed after 20 h in thiol solution (Figure S1(D), Supporting Information), Au vacancy islands are clearly observed at boundaries between ordered domains, but the β'-phase is not observed. This suggests that β'-phase formation is substrate potential-induced, i.e., the β-phase is stable and does not transform to the β'-phase without applied potential >0.3 V.

Sequential imaging of an incompletely ordered domain demonstrates that thiolates diffuse into and out of molecular rows, and order to extend the molecular row (Figure 5 A−D). This reorganization of adsorbed 4-MBT molecules in the SAMs was imaged only at potentials positive of 0.3 V, comparable to the potential of zero charge (pzc) of Au(111). We hypothesize that the reason that this surface diffusion is only observed at potentials >0.3 V is that the interaction between the sulfur and Au atoms becomes stronger with increasing potential. Positive potentials, promoting the strong adsorption of thiols to gold, can lead to diffusion of thiolate−Au complexes and formation of ordered structures as shown in Figure 5.[48−53]

Phase Transformation 2: A Function of Substrate Potential. Potential-induced structural changes of 4-MBT SAMs were observed at substrate potentials positive and negative of 0.3 V. Stepping the substrate potential from 0.4 to 0.2 V results in adsorbate islands appearing at the domain boundaries (Figure 6B). The number and the size of the islands rapidly increase, and these islands connect to each other to form a network (γ-phase) on the surface. Cross-sectional analysis (Figure 6) shows that the γ-phase island network is 2.0 ± 0.5 Å higher than the rest of the surface. Internal, molecular-scale structure can be resolved (Figure 7A). It should be noted that the apparent height in STM images reflects tunneling probabilities between adsorbate and substrate, not necessarily physical height. However, the higher packing density determined for the γ phase (vide infra), and the apparently taller structure, are consistent with a more vertical molecular orientation of 4MBT in the γ phase than in the α,β and β' phases.

The phase transformation of 4-BMT SAMs from the α-phase to the γ-phase starts at less ordered regions of the surface, e.g., α-phase domain boundaries, which is similar to thiol desorption, in that the process is initiated from the defects in the SAM such as the edges of the vacancy islands.[54] However, 4-MBT desorption probably does not take place at 0.2 V (Figure 3), and in the γ-phase 4-MBT molecules are more densely packed than in the α-phase (Figure 7B).

The average intermolecular spacing between stripes is 0.36 ± 0.02 nm, and the distance between nearest neighbor molecules in the stripe is 0.47 ± 0.01 nm (Figure S2, Supporting

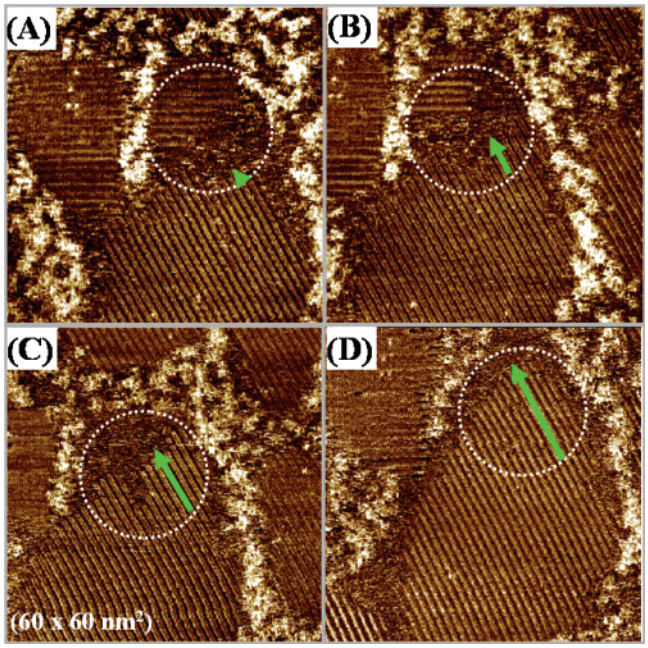

Figure 5. Sequence of STM images (A−D) showing the surface transformation of the ordered and disordered domain 4-MBT on Au(111) in 0.1 M $HClO_4$ at 0.4 V. The dotted circles indicate ordered molecular rows growing with the surface diffusion of 4-MBT−Au complexes. The tip potential and tunneling current were 0.1 V and 0.6 nA, respectively. Each image took 3 min. The 4-MBT SAM was prepared by immersion of Au(111) in 0.05 mM ethanol solution for 5 min.

Information). A possible model, a ($\sqrt{3} \times 1$) structure, corresponding to local coverage of 0.5 ML (0.69×10^{15} molecules cm^{-2}) is proposed (Figure S2C, Supporting Information). The distance (0.29 nm) between molecules in the ($\sqrt{3} \times 1$) structure is smaller than the van der Waals diameter of sulfur (0.37 nm).

One of possible explanations for the small intermolecular distances, and the formation of the ($\sqrt{3} \times 1$) structure, is that, at potentials negative of 0.3 V_{SCE}, a decrease of the interaction between 4-MBT and the substrate leads to a relative increase of intermolecular $\pi-\pi$ ring interactions.[24, 25] The stacking distance of aromatic rings in SAMs on Au(111) is influenced by intermolecular $\pi-\pi$ ring interactions. There is precedent in the literature for such tight packing in aromatic SAMs. For example, 4,4′-bypyridine formed dense packing on Au(111) with the stacking distance as short as 0.31 nm.[7] The stacking distance in 4-mercapropyridine SAMs on Au(111) decreased from a ($5 \times \sqrt{3}$) to a ($\sqrt{3} \times 1$) structure as substrate potential changed from 0.4 to 0.15 V.[24,25] In the ($\sqrt{3} \times 1$) structure, the S−S distance of 0.32 ± 0.05 nm was reported for 4-mercaptopyridine (4-MPY) SAMs on Au(111).[24,25] This structure corresponds to a coverage of 0.5 ML, and provides a precedent for our assignment of a 0.5 ML coverage for the γ-phase. While an anion network might drive charged 4-MPY molecules to order with the ($\sqrt{3} \times 1$) structure in H_2SO_4, there is no reason for anions to play the same role with uncharged 4-MBT molecules. However, 4-MBT does apparently form a ($\sqrt{3} \times 1$) structure. This suggests that intermolecular interactions need to be considered as explanations for the high coverage structures of 4-MPY.[24,25]

Another possible suggestion for the small intermolecular distances is the sulfur−sulfur dimerization at thiolate headgroups.[27,55] The dimerization at the sulfur headgroups for the decanethiol[55] and 4-mercaptopyridine[27] SAMs on Au(111) led to a sulfur−sulfur spacing of 0.21−0.22 nm. We suggest that at potentials negative of 0.3 V, a decrease of the interaction between 4-MBT and the substrate could drive the thiolate headgroups to form weak dimers. This process could lead to the S−S distance being smaller than the van der Waals diameter of sulfur.

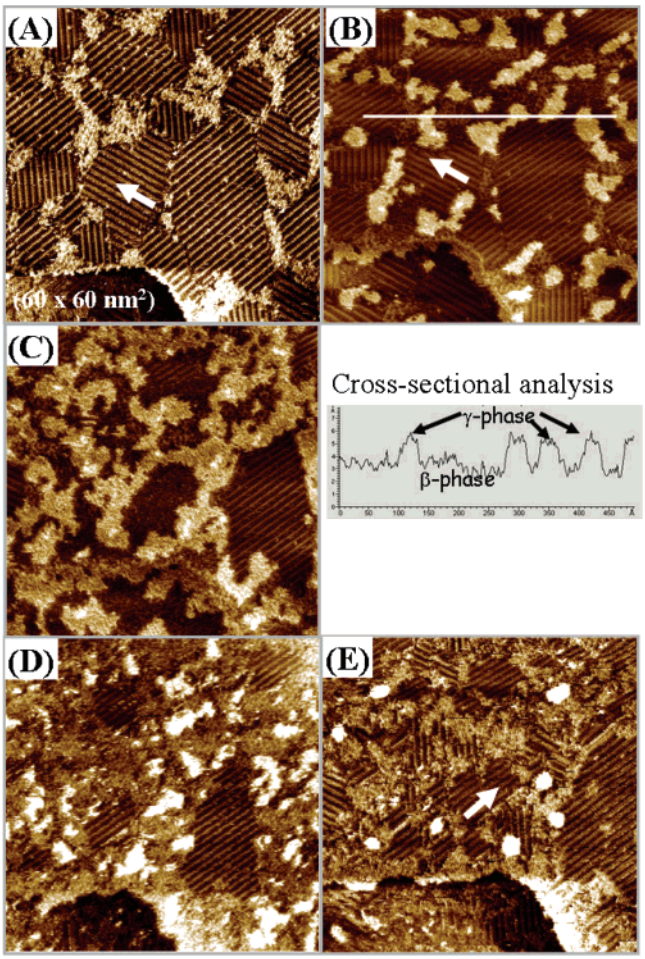

Figure 6. Time-lapse images of the 4-MBT SAM on Au(111) in 0.1 M $HClO_4$ showing phase transformation with different substrate potentials: (A) substrate potential (V_{sub}) = 0.4 V, tunneling current (I_t) = 0.4 nA; (B, C) V_{sub} = 0.2 V, I_t = 0.1 nA; and (D, E) V_{sub} = 0.4 V, I_t = 0.4 nA. The STM tip potential was 0.1 V. The 4-MBT SAM was prepared by immersion of Au(111) in 0.2 mM ethanol solution for 5 min. Imaging conditions: (A) after holding at 0.4 V for ~2 h, (B, C) after imaging at 0.2 V for 7 and 21 min, respectively; and (D, E) after stepping a potential from 0.2 to 0.4 V and imaging at 0.4 V for 10 and 50 min, respectively. (D) An intermediate surface structure as the system undergoes reverse phase transformation from γ-phase to α-phase; the brighter areas indicate the γ-phase. White arrows indicate a different direction of molecular rows.

When the substrate potential is stepped back from 0.2 to 0.4 V, the γ-phase network turns into a disordered intermediate phase, showing the reversibility of the α-phase ↔ γ-phase transformation, as the potential is driven positive and negative of 0.3 V (Figure 6D). Subsequently, the disordered molecules start to form ordered molecular rows (α-phase) (Figure 6E). The new striped structures are oriented in directions different from the structures in Figure 6A. While the stripe direction in Figure 6E reflects the crystallographic threefold symmetry of Au(111), the particular direction (120°, 240°, or 360°) is random and can change as the system is driven through a α-phase to γ-phase to α-phase transformation.

In addition to substrate potential-induced ordering of the 4-MBT SAM, at potentials positive of 0.3 V, a shape change of monatomic depth vacancies reveals surface diffusion of 4-MBT−Au complexes rather than bare thiolates (Figure S3,

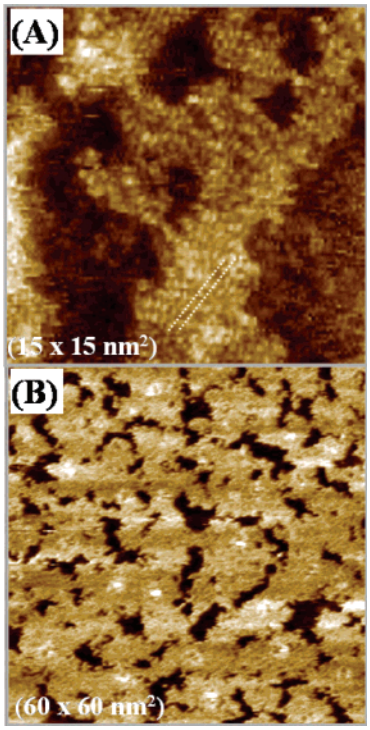

Figure 7. STM images of the γ-phase in 0.1 M $HClO_4$: (A) substrate potential (V_{sub}) = 0.2 V, tip potential (V_{tip}) = 0.1 V, and tunneling current (I_t) = 0.1 nA; (B) V_{sub} = 0.2 V, V_{tip} = −0.05 V, and I_t = 0.1 nA. The dotted line in part A indicates stripes. Dark regions in (B) are holes about 2 Å deep. The 4-MBT SAM was prepared by immersion of Au(111) in 0.2 mM ethanol solution for 5 min.

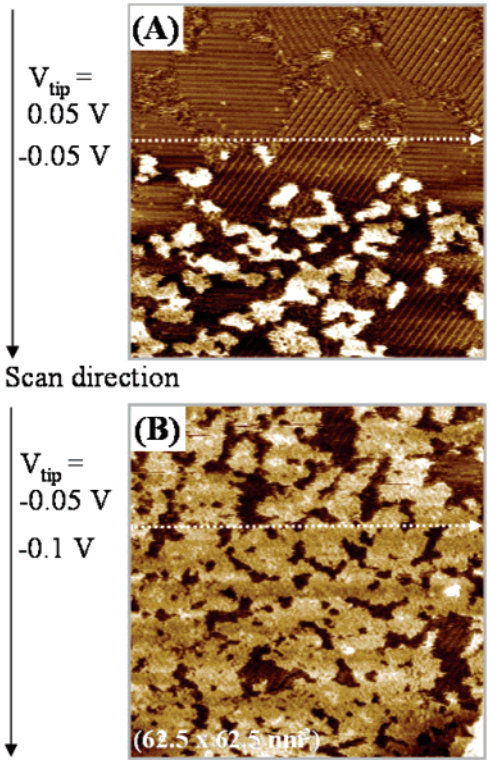

Figure 8. Images of the 4-MBT SAM on Au(111) in 0.1 M $HClO_4$ showing the effect of tip potential on phase transformation; at the dotted white line, the tip potential is stepped (A) from 0.05 to −0.05 V and (B) from −0.05 to −0.1 V. The 4-MBT SAM was prepared by immersion of Au(111) in 0.2 mM ethanol solution for 5 min. The substrate potential and tunneling current were 0.2 V and 0.2 nA, respectively.

Supporting information). Bare thiolate diffusion alone should not cause changes in the underlying substrate (i.e., the hole). Therefore, we suggest that, at potentials positive of 0.3 V, ordering of 4-MBT SAM, e.g., phase transformation from the β-phase to β'-phase including Ostwald ripening of α-phase domains, is mediated by diffusion of 4-MBT−Au complexes. The ($2\sqrt{3} \times \sqrt{3}$) and ($4 \times \sqrt{3}$) structures observed in the α-phase correspond to local coverages of 0.33 and 0.25 ML, respectively. The β'-phase, a (3×3) structure, corresponds to a local coverage of 0.19 ML. These values are low compared to the surface concentration determined by CV. We suggest that the aggregated molecules of the β-phase are a source of thiols that order into the α- and β'-phase.

Effect of Concentration. While our investigation focused on the effect of potential on molecular ordering or disordering, we did investigate the effect of concentration briefly. To probe the initial state of SAMs, the Au(111) substrate was immersed for short time (5 min) in 0.05−0.2 mM 4-MBT in ethanol. However, because a relatively long scanning time was necessary for stable STM images to be observed, it was hard to judge the degree of order of samples prepared for 5 min at different concentrations which form ordered structures under potential control. Nevertheless, there was no noticeable effect of concentration on the phase transformation between disordered and ordered structures.

Phase Transformation 3: A Function of Tip Potential. The observation of a ($\sqrt{3} \times 1$) structure (γ-phase) and a ($4 \times \sqrt{3}$) structure (α-phase) for 4-MBT is similar to previous reports for 4-MPY.[25,39] In our STM experiments, however, a significant effect of the tip-induced electric field on the phase transformation was observed in 4-MBT SAMs at potentials negative of 0.3 V. The γ-phase of 4-MBT SAMs is observed only in the vicinity of a scanned area but not over the entire surface. The zoomed-out image (Figure S4, Supporting Information) shows a phase-transformed surface that is larger and different in shape (circle) compared to the scanned square area (square). This image provides clear evidence that the tip can trigger the surface phase transformations. A phase transformed area that is larger than the scanned area suggests that the phase transformation is a consequence of the interaction between the electric field of the tip and the 4-MBT−substrate complexes rather than physical deformation of the SAM by the STM tip.

In the course of this local phase transformation from the α-phase to the γ-phase, many holes about 2 Å deep are observed in the γ-phase. For the phase transformation from the α-phase to the γ-phase, adsorption or desorption of 4-MBT does not occur in the potential window explored in the STM measurements. Therefore, we suggest that packing density in the γ-phase of 4-MBT molecules is larger than the α-phase, so that, in the absence of a total coverage change, the locally increased molecular packing density leads to the formation of holes.

At a substrate potential of 0.2 V, the γ-phase suddenly appears after stepping the tip potential from 0.05 to −0.05 V (Figure 8A). Stepping the tip bias to such negative potentials accelerates the transformation from the α-phase to the γ-phase. We speculate that the tip electric field perturbs the molecular charge distribution and is more effective on the weaker sulfur−Au bond that prevails at potentials negative of the PZC. The transformation from the α-phase to the γ-phase is probably triggered by tip−surface electrostatic interactions, affecting the stability of the 4-MBT SAM structure. The negatively polarized tip clearly influences the kinetics of the process, (Figure 8) presumably by assisting the mobility of the 4-MBT. The driving force for self-assembly, the intermolecular $\pi-\pi$ interaction between benzene rings, is, to first order, potential independent. The $\pi-\pi$

stacking distance of two aromatic rings is reported to be 3.3 Å,[8] consistent with the distance observed between molecular rows in the γ-phase. A change in the relative magnitude of headgroup−substrate interactions and molecule−molecule interactions, i.e., decrease in the former relative to the latter, drives the thiolates to form a new lattice whose structure is determined by the intermolecular $\pi-\pi$ interaction.

This speculation is based on the observation that the phase transformations of 4-MBT SAM are different from those of 4-MPY SAM. The 4-MPY SAM in 0.1 M $HClO_4$ does not show a potential-induced structural transformation, whereas in 0.1 M H_2SO_4 the phase transition is observed.[25]

In light of the α-phase to the γ-phase transition for 4-MBT, we performed similar experiments, in 0.1 M $HClO_4$, on the charged 4-MPY. The initial motivation was to explore mechanical tip perturbations of the SAM. Under the conditions we employed, 4-MPY does not undergo the phase transformation (Figure S5, Supporting Information), while the uncharged 4-MBT can. Our hypothesis, related to the ability of the sulfate anion, and inability of perchlorate, to "specifically adsorb",[56] is that the protonated terminal nitrogen moiety of 4-MPY is associated with anions in H_2SO_4 but not in $HClO_4$ solution,[24,25] suggesting that effective neutralization of the charged terminal of the molecules, rather than the negative charge of the surface, drives the transformation. The "neutral" 4-MPY can undergo the phase transition, whereas the "charged" 4-MPY cannot, presumably because repulsive interactions prevent formation of a more tightly packed phase. It appears, therefore, that the tip effect is greater for uncharged aromatic thiols such as 4-MBT.

Conclusion

The strong interaction between aromatic rings drives adsorbed 4-MBT molecules to form ordered structures (α-phase) with aggregated molecular patches (β-phase) at the boundaries of ordered domains.

At potentials positive of 0.3 V, an ordered β'-phase appears at striped α-phase domain boundaries. At potentials negative of 0.3 V, a tip-enhanced phase transformation leads to the appearance of a new phase (γ-phase) in the scanned area. The γ-phase reversibly reorders to form striped structures via intermediate disordering after stepping to a potential positive of the pzc. Our results suggest that, at potentials positive of 0.3 V, an increase in the binding strength of thiolate to Au leads to potential-induced structural transformations from the β-phase to the β'-phase and from the γ-phase to the α-phase. These effects are mediated by diffusion of 4-MBT−Au complexes. However, at potentials negative of 0.3 V, a potential-induced structural transformation from the α-phase to the γ-phase of 4-MBT SAMs is explained by a decrease of adsorbate−substrate binding.

Acknowledgment. This work was supported by the NSF (CHE 0456965). K.S. acknowledges the partial support of the Postdoctoral Fellowship Program of the Korea Science & Engineering Foundation (KOSEF).

Supporting Information Available: STM images of potential-annealed and solution-annealed 4-MBT SAMs (S1); STM images of the internal structure of γ-phase and the proposed model structure (S2); STM images showing change in the shape of monatomic depth vacancies (S3); STM images revealing tip-potential enhanced transformations (S4); and STM images for the 4-mercaptopyridine SAM on Au(111) (S5). This material is available free of charge via the Internet at http://pubs.acs.org.

References and Notes

(1) Ulman, A. *Chem. Rev.* **1996**, *96*, 1533.
(2) Nuzzo, R. G.; Allara, D. L. *J. Am. Chem. Soc.* **1983**, *105*, 4481.
(3) Dubois, L. H.; Nuzzo, R. G. *Annu. Rev. Phys. Chem.* **1992**, *43*, 437.
(4) Porter, M. D.; Bright, T. B.; Allara, D. L.; Chidsey, C. E. D. *J. Am. Chem. Soc.* **1987**, *109*, 3559.
(5) Jin, Q.; Rodriguez, J. A.; Li, C. Z.; Darici, Y.; Tao, N. J. *Surf. Sci.* **1999**, *425*, 101.
(6) Cunha, F.; Jin, Q.; Tao, N. J.; Li, C. Z. *Surf. Sci.* **1997**, *389*, 19.
(7) Cunha, F.; Tao, N. J.; Wang, X. W.; Jin, Q.; Duong, B.; Dagnese, J. *Langmuir* **1996**, *12*, 6410.
(8) Cunha, F.; Tao, N. J. *Phys. Rev. Lett.* **1995**, *75*, 2376.
(9) Bumm, L. A.; Arnold, J. J.; Cygan, M. T.; Dunbar, T. D.; Burgin, T. P.; Jones, L.; Allara, D. L.; Tour, J. M.; Weiss, P. S. *Science* **1996**, *271*, 1705.
(10) Tour, J. M.; Jones, L.; Pearson, D. L.; Lamba, J. J. S.; Burgin, T. P.; Whitesides, G. M.; Allara, D. L.; Parikh, A. N.; Atre, S. V. *J. Am. Chem. Soc.* **1995**, *117*, 9529.
(11) Sawaguchi, T.; Mizutani, F.; Yoshimoto, S.; Taniguchi, I. *Electrochim. Acta* **2000**, *45*, 2861.
(12) Cyganik, P.; Buck, M.; Azzam, W.; Woll, C. *J. Phys. Chem. B* **2004**, *108*, 4989.
(13) Dhirani, A. A.; Zehner, R. W.; Hsung, R. P.; GuyotSionnest, P.; Sita, L. R. *J. Am. Chem. Soc.* **1996**, *118*, 3319.
(14) Yang, G. H.; Qian, Y. L.; Engtrakul, C.; Sita, L. R.; Liu, G. Y. *J. Phys. Chem. B* **2000**, *104*, 9059.
(15) Ishida, T.; Mizutani, W.; Choi, N.; Akiba, U.; Fujihira, M.; Tokumoto, H. *J. Phys. Chem. B* **2000**, *104*, 11680.
(16) Fuxen, C.; Azzam, W.; Arnold, R.; Witte, G.; Terfort, A.; Woll, C. *Langmuir* **2001**, *17*, 3689.
(17) Yang, G. H.; Liu, G. Y. *J. Phys. Chem. B* **2003**, *107*, 8746.
(18) Baunach, T.; Kolb, D. M. *Anal. Bioanal. Chem.* **2002**, *373*, 743.
(19) Tao, Y. T.; Wu, C. C.; Eu, J. Y.; Lin, W. L.; Wu, K. C.; Chen, C. H. *Langmuir* **1997**, *13*, 4018.
(20) Nara, J.; Higai, S.; Morikawa, Y.; Ohno, T. *J. Chem. Phys.* **2004**, *120*, 6705.
(21) Batz, V.; Schneeweiss, M. A.; Kramer, D.; Hagenstrom, H.; Kolb, D. M.; Mandler, D. *J. Electroanal. Chem.* **2000**, *491*, 55.
(22) Nielsen, J. U.; Esplandiu, M. J.; Kolb, D. M. *Langmuir* **2001**, *17*, 3454.
(23) Wan, L. J.; Terashima, M.; Noda, H.; Osawa, M. *J. Phys. Chem. B* **2000**, *104*, 3563.
(24) Zhou, W. P.; Baunach, T.; Ivanova, V.; Kolb, D. M. *Langmuir* **2004**, *20*, 4590.
(25) Baunach, T.; Ivanova, V.; Scherson, D. A.; Kolb, D. A. *Langmuir* **2004**, *20*, 2797.
(26) Wan, L. J.; Noda, H.; Hara, Y.; Osawa, M. *J. Electroanal. Chem.* **2000**, *489*, 68.
(27) Wan, L. J.; Hara, Y.; Noda, H.; Osawa, M. *J. Phys. Chem. B* **1998**, *102*, 5943.
(28) Sawaguchi, T.; Mizutani, F.; Taniguchi, I. *Langmuir* **1998**, *14*, 3565.
(29) Trevor, D. J.; Chidsey, C. E. D.; Loiacono, D. N. *Phys. Rev. Lett.* **1989**, *62*, 929.
(30) Sette, F.; Hashizume, T.; Comin, F.; Macdowell, A. A.; Citrin, P. H. *Phys. Rev. Lett.* **1988**, *61*, 1384.
(31) Wetterer, S. M.; Lavrich, D. J.; Cummings, T.; Bernasek, S. L.; Scoles, G. *J. Phys. Chem. B* **1998**, *102*, 9266.
(32) Lavrich, D. J.; Wetterer, S. M.; Bernasek, S. L.; Scoles, G. *J. Phys. Chem. B* **1998**, *102*, 3456.
(33) Whelan, C. M.; Barnes, C. J.; Gregoire, C.; Pireaux, J. J. *Surf. Sci.* **2000**, *454*, 67.
(34) Kondoh, H.; Kodama, C.; Sumida, H.; Nozoye, H. *J. Chem. Phys.* **1999**, *111*, 1175.
(35) Kondoh, H.; Kodama, C.; Nozoye, H. *J. Phys. Chem. B* **1998**, *102*, 2310.
(36) Ishida, T.; Fukushima, H.; Mizutani, W.; Miyashita, S.; Ogiso, H.; Ozaki, K.; Tokumoto, H. *Langmuir* **2002**, *18*, 83.
(37) McCarley, R. L.; Dunaway, D. J.; Willicut, R. J. *Langmuir* **1993**, *9*, 2775.
(38) Schweizer, M.; Hagenstrom, H.; Kolb, D. M. *Surf. Sci.* **2001**, *490*, L627.
(39) Hagenstrom, H.; Schneeweiss, M. A.; Kolb, D. M. *Langmuir* **1999**, *15*, 2435.
(40) Kolb, D. M.; Schneider, J. *Electrochim. Acta* **1986**, *31*, 929.
(41) Stipe, B. C.; Rezaei, M. A.; Ho, W. *J. Chem. Phys.* **1997**, *107*, 6443.
(42) Lyo, I. W.; Avouris, P. *Science* **1991**, *253*, 173.
(43) Touzov, I.; Gorman, C. B. *J. Phys. Chem. B* **1997**, *101*, 5263.
(44) He, Y.; Borguet, E. *J. Phys. Chem. B* **2001**, *105*, 3981.
(45) Poirier, G. E. *Langmuir* **1997**, *13*, 2019.

(46) Byloos, M.; Al-Maznai, H.; Morin, M. *J. Phys. Chem. B* **1999**, *103*, 6554.
(47) Walczak, M. M.; Popenoe, D. D.; Deinhammer, R. S.; Lamp, B. D.; Chung, C. K.; Porter, M. D. *Langmuir* **1991**, *7*, 2687.
(48) Bretz, R. L.; Abruna, H. D. *J. Electroanal. Chem.* **1995**, *388*, 123.
(49) Cohen-Atiya, M.; Mandler, D. *J. Electroanal. Chem.* **2003**, *550*, 267.
(50) Ma, F. Y.; Lennox, R. B. *Langmuir* **2000**, *16*, 6188.
(51) Paik, W. K.; Eu, S.; Lee, K.; Chon, S.; Kim, M. *Langmuir* **2000**, *16*, 10198.
(52) Yang, Y. C.; Yen, Y. P.; Yang, L. Y. O.; Yau, S. L.; Itaya, K. *Langmuir* **2004**, *20*, 10030.
(53) Muskal, N.; Mandler, D. *Electrochim. Acta* **1999**, *45*, 537.
(54) Wano, H.; Uosaki, K. *Langmuir* **2001**, *17*, 8224.
(55) Fenter, P.; Eberhardt, A.; Eisenberger, P. *Science* **1994**, *266*, 1216.
(56) Kolb, D. M. *Prog. Surf. Sci.* **1996**, *51*, 109.